A Complex-LASSO Approach for Localizing Forced Oscillations in Power Systems

Rajasekhar Anguluri, Nima Taghipourbazargani, Oliver Kosut, and Lalitha Sankar
School of Electrical, Computer, and Energy Engineering
Arizona State University, Tempe, AZ 85281 USA
{rangulur,ntaghip1,okosut,lalithasankar}@asu.edu

***Abstract*—We study the problem of localizing multiple sources of forced oscillations (FOs) and estimating their characteristics, including frequency, phase, and amplitude, using noisy PMU data. We assume sparsity in the number of locations, and for each location, we model the input FO as a sum of a few unknown sinusoids. This allows us to obtain a sparse linear model in the frequency domain that relates measurements and the unknown input locations at frequencies of the unknown sinusoidal terms. We determine these frequencies by thresholding the empirical spectrum of the noisy data. Finally, we cast the location recovery problem as an ℓ_1-regularized least squares problem in the complex domain—i.e., complex-LASSO (linear shrinkage and selection operator). We numerically solve this optimization problem using the complex-valued coordinate descent method and show its efficiency on the IEEE 68-bus, 16 machine and WECC 179-bus, 29-machine systems.**

***Index Terms*—Forced oscillations, complex-LASSO, sparsity, sampled data system, PMU measurements.**

I. Introduction

Detecting and localizing forced oscillations (FOs) is crucial for safety and reliability of power systems. Detection helps determine if the manifested oscillations in PMU measurements are FOs; whereas localization helps to mitigate the oscillations either by disabling the sources (e.g., malfunctioned controllers and cyclic loads) or by injecting certain counteracting signals [1]. Compared to localization, detecting oscillations is easier and has been well studied in power systems [2].

We focus on localizing the sources of FO, which amounts to finding m^* true sources from m possible sources. A brute-force search requires searching across $\binom{m}{m^*}$ configurations, which is prohibited for large m. One way to address this problem is to find locations that optimizes measures, such as $\mathcal{H}_2$/$\mathcal{H}_\infty$ norms and information-theoretic based measures [3]. Instead, by leveraging the fact that the FO sources are sparse ($m^* \ll m$) [1], [4], we find the locations and the associated input parameters using an ℓ_1-norm regularized optimization problem. In several sparse inverse problems—finding unknown sparse parameters using a few measurements—ℓ_1-norm regularization has shown to accurately recover the sparsity pattern of the unknown parameter than the ℓ_2-norm regularization [5]. Sparsity has been long recognized in power systems, especially in state and topology estimation problems; however, sparsity methods are less explored for localizing FO sources [6].

This material is based upon work supported by the National Science Foundation under Grant No. OAC-1934766 and PSERC project S-87.

Using the standard discrete time Fourier transform (DTFT), we obtain the complex-valued linear model $\mathbf{Y}_K = \mathbf{H}_K \mathbf{U}_K$, where K is the total number of sinusoidal frequencies at all locations; $\mathbf{H}_K$ is a block-diagonal matrix of transfer functions, each evaluated at the unknown sinusoidal frequency; and $\mathbf{Y}_K$ is the measurement in the Fourier domain corresponding to the K unknown input frequencies. Finally, $\mathbf{U}_K$ jointly[1] encodes sparsity in the number of locations and the number of sinusoids (see In Section II for details). For the above linear model, we summarize our location recovery method below:

1) First, we use the fast Fourier transform (FFT) to determine these K frequencies by thresholding the spectrum of measurements collected over a finite time interval.
2) Second, for the model $\mathbf{Y}_K = \mathbf{H}_K \mathbf{U}_K$, we solve an ℓ_1 regularized least squares (henceforth, LASSO) problem in the complex domain via coordinated descent method [8] to infer: (i) the number of true locations and the number of sinusoids at any given location, and (ii) the frequency, phase, and amplitude of each sinusoid.

Our recovery algorithm is simple as it requires thresholding the spectrum and solving a convex optimization problem. We validate its performance on two benchmark systems.

Related literature: In [9]–[11], sources were identified using spectral properties of the transfer functions between sources and measurements. Instead, by representing generators' frequency response as an effective admittance matrix and oscillations as current injections, [12] identifies sources by comparing predicted against measured current spectrum, and [13] uses a Bayesian approach. Finally, in [6], a sparse plus low rank decomposition of Hankel measurement matrices has been suggested to localize the sources.

However, unlike our method, algorithms in the above studies localize sources (mostly single, i.e., $m^* = 1$) but do not jointly estimate the input. Further, with the exception of works in [6] and [13], sparsity has not been explored in a systematic way. The work closest to ours is [13], which considers an ℓ_1-norm regularized optimization framework in a Bayesian setting. However, [13] models FOs as current injections and generators as frequency response functions. Instead, we model FOs as exogenous inputs, which could be genuine oscillations, malicious attacks, faults, or unmodeled dynamics. Thus, our

[1]This kind of joint sparsity might not be possible in the time-domain, especially, for arbitrary forced inputs [7].

Israel-US BIRD Foundation

978-1-6654-0823-3/22/$31.00 ©2022 IEEE

modeling framework and the subsequent optimization procedure apply to find any form of disturbances in dynamical systems, including in power systems that are modeled using descriptor models[2]. Moreover, we consider practical aspects, including spectral leakage and the measurement.

II. System dynamics under forced oscillations

Consider the following linearized multi-machine dynamics excited by external unknown inputs in state-space form:

$$\dot{\mathbf{x}}(t) = \mathbf{A}\mathbf{x}(t) + \mathbf{B}\mathbf{u}(t), \quad \mathbf{y}(t) = \mathbf{C}\mathbf{x}(t), \quad \forall t \geq 0. \tag{1}$$

The state vector $\mathbf{x}(t) \in \mathbb{R}^n$ includes machine internal dynamics and variables associated with closed-loop controllers. We model the input $\mathbf{u}(t) \in \mathbb{R}^m$ as the forced oscillation vector:

$$\mathbf{u}(t) \triangleq \begin{bmatrix} u_1(t) \\ u_2(t) \\ \vdots \\ u_m(t) \end{bmatrix} = \begin{bmatrix} \sum_{l=1}^{M_1} a_{1,l} \sin(\omega_{1,l} t + \phi_{1,l}) \\ \sum_{l=1}^{M_2} a_{2,l} \sin(\omega_{2,l} t + \phi_{2,l}) \\ \vdots \\ \sum_{l=1}^{M_m} a_{m,l} \sin(\omega_{m,l} t + \phi_{m,l}) \end{bmatrix} \tag{2}$$

where $a_{r,l} \geq 0$, $\omega_{r,l} = 2\pi f_{r,l} \geq 0$, and $\phi_{r,l}$ are the amplitude, angular frequency, and phase of the l^{th} sinusoid term at the r^{th} location, and $r \in \{1, \ldots, m\}$. Finally, $\mathbf{y}(t) \in \mathbb{R}^p$ is the measurement obtained from p sensors. For simplicity, we build the theory using noise-free measurements, and later consider measurement noise in simulations.

By modeling forced input as a sum of multiple weighted sinusoids, we allow for different oscillatory waveforms. Thus, our approach generalizes the approaches recovering a single sinusoidal input, which are well studied in the literature [1], [4]. Let $\mathbf{a}_r(t) = [a_{r,1} \sin(\omega_{r,1} t + \phi_{r,1}) \cdots a_{r,M_r} \sin(\omega_{r,M_r} t + \phi_{r,M_r})]$ be the vector of sinusoids at the r^{th} location. We make the following assumption on $\mathbf{u}(t)$ in (1) and $\mathbf{a}_r(t)$.

Assumption 1: Both $\mathbf{u}(t)$ in (1) and $\mathbf{a}_r(t)$ defined above are sparse; that is, $\|\mathbf{u}(t)\|_0 \ll m$ and $\|\mathbf{a}_r(t)\|_0 \ll M_r$, where $\|\mathbf{z}\|_0$ counts the number of non-zero entries in the vector $\mathbf{z}$.

As PMUs record measurements at discrete time instants, we sample (1) with the sampling period T (e.g., $F = 1/T = 30$–60 Hz for PMUs). Let $\mathbf{A}_d = \exp(\mathbf{A}T)$ and $\mathbf{B}_d = \int_0^T \exp(\mathbf{A}(T-s))ds\,\mathbf{B}$. Let $k = 0, 1, \ldots$ and define $\mathbf{x}[k] \triangleq \mathbf{x}(kT)$, $\mathbf{u}[k] \triangleq \mathbf{u}(kT)$, and $\mathbf{y}[k] \triangleq \mathbf{y}(kT)$. Suppose that $\mathbf{u}(t)$ is a piecewise constant[3] during $kT \leq t \leq (k+1)T$. Then

$$\mathbf{x}[k+1] = \mathbf{A}_d \mathbf{x}[k] + \mathbf{B}_d \mathbf{u}[k], \quad \mathbf{y}[k] = \mathbf{C}\mathbf{x}[k] \tag{3}$$

describe the discrete-time sampled model of (1). As our focus is on oscillations triggered by inputs, we assume $\mathbf{x}[0] = \mathbf{0}$.

Define the matrix-valued transfer function $\mathbf{H}[z] = \mathbf{C}(z\mathbf{I} - \mathbf{A}_d)^{-1}\mathbf{B}_d \in \mathbb{C}^{p \times m}$, where $z \in \mathbb{C}$. Then, from the standard linear system analysis, we conclude that $\mathbf{Y}[z] = \mathbf{H}[z]\mathbf{U}[z]$, where $\mathbf{Y}[z] \in \mathbb{C}^{p \times 1}$ and $\mathbf{U}[z] \in \mathbb{C}^{m \times 1}$ are the Z-transforms of $\mathbf{y}[k]$ and $\mathbf{u}[k]$. Finally, at $z = \exp(j\Omega)$, where $\Omega \in (0, 2\pi)$ and $j^2 = -1$, we have the DTFT representation of (3):

$$\mathbf{Y}[e^{j\Omega}] = \mathbf{H}[e^{j\Omega}]\mathbf{U}[e^{j\Omega}]. \tag{4}$$

[2]Descriptor models can allow us to model disturbances in loads and FACTS based devices. However, for simplicity, we do not study these models.

[3]Frequencies of real FOs are smaller than the sampling frequency of PMUs.

The benefit of working in the Fourier (or frequency) domain is that $\mathbf{U}[e^{j\Omega}]$ can be expressed as a sum of weighted Dirac delta functions. As a result, $\mathbf{Y}[e^{j\Omega}]$ can be expanded in terms of basis functions that encode both the source location and frequency of the input sinuosoids. Using this observation, we later show that the source localization problem can be cast as a solution to a simple ℓ_1 regularized least-squares problem.

Since $\mathbf{u}(t)$ in (2) is a sum of sinusoids, it follows that

$$\mathbf{U}[e^{j\Omega}] = j\pi \begin{bmatrix} \sum_{l=1}^{M_1} a_{1,l}\, e^{j\phi_{1,l}} [\delta(\Omega + \widetilde{\omega}_{1,l}) - \delta(\Omega - \widetilde{\omega}_{1,l})] \\ \sum_{l=1}^{M_2} a_{2,l}\, e^{j\phi_{2,l}} [\delta(\Omega + \widetilde{\omega}_{2,l}) - \delta(\Omega - \widetilde{\omega}_{2,l})] \\ \vdots \\ \sum_{l=1}^{M_m} a_{m,l}\, e^{j\phi_{m,l}} [\delta(\Omega + \widetilde{\omega}_{m,l}) - \delta(\Omega - \widetilde{\omega}_{m,l})] \end{bmatrix} \tag{5}$$

where $\delta(x)$ is the Dirac delta function and $\widetilde{\omega}_{k,l} = \omega_{k,l} T$. Note that $\mathbf{U}[e^{j\Omega}]$ is non-zero only for $\Omega \in \{\pm\widetilde{\omega}_{1,1}, \ldots, \pm\widetilde{\omega}_{m,M_m}\}$. Suppose that for Ω in this set, $\mathbf{H}[e^{j\Omega}] \neq \mathbf{0}$. Then, from (4), we have $\mathbf{Y}[e^{j\Omega}] \neq \mathbf{0}$. If this is not the case, we cannot recover the sinusoid oscillating with Ω using measurements. Finally, we have $\mathbf{Y}[e^{j\Omega}] = \mathbf{Y}^*[e^{-j\Omega}]$. Thus, we focus only on $\widetilde{\omega}_{k,l} \geq 0$.

With a slight abuse of notation, let $\{\widetilde{\omega}_1, \ldots, \widetilde{\omega}_K\}$ be the set of frequencies where $\mathbf{Y}[e^{j\widetilde{\omega}_l}] = \mathbf{H}[e^{j\widetilde{\omega}_l}]\mathbf{U}[e^{j\widetilde{\omega}_l}] \neq \mathbf{0}$, where both $\widetilde{\omega}_l$ and K are unknown. Consider the following model:

$$\underbrace{\begin{bmatrix} \mathbf{Y}[e^{j\widetilde{\omega}_1}] \\ \mathbf{Y}[e^{j\widetilde{\omega}_2}] \\ \vdots \\ \mathbf{Y}[e^{j\widetilde{\omega}_K}] \end{bmatrix}}_{\triangleq \mathbf{Y}_K} = \underbrace{\begin{bmatrix} \mathbf{H}[e^{j\widetilde{\omega}_1}] & & & \\ & \mathbf{H}[e^{j\widetilde{\omega}_2}] & & \\ & & \ddots & \\ & & & \mathbf{H}[e^{j\widetilde{\omega}_K}] \end{bmatrix}}_{\triangleq \mathbf{H}_K} \underbrace{\begin{bmatrix} \mathbf{U}[e^{j\widetilde{\omega}_1}] \\ \mathbf{U}[e^{j\widetilde{\omega}_2}] \\ \vdots \\ \mathbf{U}[e^{j\widetilde{\omega}_K}] \end{bmatrix}}_{\triangleq \mathbf{U}_K} \tag{6}$$

where $\mathbf{Y}_K \in \mathbb{C}^{pK \times 1}$, $\mathbf{H}_K \in \mathbb{C}^{pK \times mK}$, and $\mathbf{U}_K \in \mathbb{C}^{mK \times 1}$. In light of Assumption 1, note that $K \ll [M_1 + \ldots + M_m]$. Further, the non-zero components of $\mathbf{U}[e^{j\widetilde{\omega}_l}] \in \mathbb{C}^m$ correspond to locations with the inputs containing sinusoids of frequency $\widetilde{\omega}_l$. Thus, from the sparsity pattern of $\mathbf{U}_K$ alone we can determine source locations and their sinusoidal frequencies (see Fig. 1). The values of $\mathbf{U}_K$ provide phase and amplitude information.

The model in (6) captures the relationship between measurements and the input locations at multiple frequencies; thus, for a sinusoid input, i.e., $\mathbf{U}[e^{j\widetilde{\omega}_l}]$ is a delta function, $\mathbf{Y}[e^{j\widetilde{\omega}_l}]$ is infinite for any l. This is a natural aspect of taking DTFTs of infinite time-length sinusoids. However, in practice, we only use measurements for a finite time interval and use FFTs to compute $\mathbf{Y}[e^{j\widetilde{\omega}_l}]$, which is consequently finite.

III. Complex-LASSO for Source Localization

In practice, the total number of sensors (p) could be less than the possible number of sources (m). For example, PMUs can measure only bus level quantities but not the internal signals of control devices. Thus, model in (6) is an under-determined system and we cannot obtain $\mathbf{U}_K$ by means of ordinary least squares. As a result, for the model in (6), we consider the ℓ_1-

Israel IS BIRD Foundation

978-1-6654-0823-3/22/$31.00 ©2022 IEEE

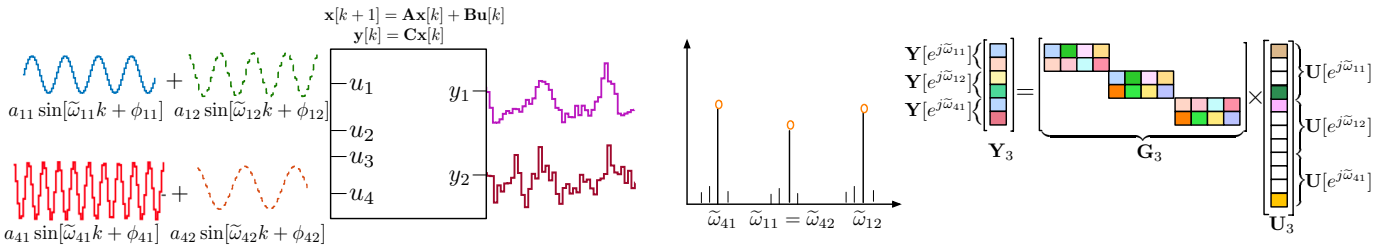

(a) power dynamics excited by forced oscillations (b) one sided amplitude spectrum of $\mathbf{Y}_3$ (c) visualization of linear model in Eq (6)

Fig. 1. (a) shows the discrete-time power system model with $m = 4$ possible locations but only locations 1 and 4 are injecting oscillations. Each of these inputs is a sum of two sinusoids with different parameters except for $\widetilde{\omega}_{11} = \widetilde{\omega}_{42}$. In Fig. (b), input frequencies are found by computing the spectrum of the two sensory measurements. Since $\widetilde{\omega}_{11} = \widetilde{\omega}_{42}$, we see only three dominant peaks in the spectrum, i.e., $K = 3$, and the smaller peaks are due to spectral leakage. In Fig. (c), we visualize linear model in (6). For any $\widetilde{\omega}_{k,l}$, the four entries (square blocks) in $\mathbf{U}[e^{j\widetilde{\omega}_{k,l}}]$ correspond to four possible locations. Locations having sinusoid oscillating with $\widetilde{\omega}_{k,l}$ are highlighted in color. The top input $\mathbf{U}[e^{j\widetilde{\omega}_{1,1}}]$ has two non-zero entries (highlighted in brown and green) indicating that locations 1 and 4 have a sinusoid with $\widetilde{\omega}_{1,1} = \widetilde{\omega}_{4,2}$.

regularized optimization problem to both localize the sources and identify the frequencies of the sinusoids at each source:

$$\widehat{\mathbf{U}}_K = \underset{\mathbf{U}_K \in \mathbb{C}^{mK\times 1}}{\arg\min} \left\{ \frac{1}{2} \|\mathbf{Y}_K - \mathbf{H}_K \mathbf{U}_K\|_2^2 + \lambda \|\mathbf{U}_K\|_1 \right\} \quad (7)$$

where $\lambda \geq 0$ is the tuning parameter. For the vector $\mathbf{z}$, the ℓ_1-norm is $\|\mathbf{z}\|_1 = \sum_i |z_i|$, where $|z_i| = \sqrt{\mathrm{Re}(z_i)^2 + \mathrm{Im}(z_i)^2}$. The regularization term $\|\mathbf{U}_K\|_1$ promotes sparsity in $\widehat{\mathbf{U}}_K$. We henceforth refer to the problem in (7) as the complex-LASSO.

Akin to $\mathbf{U}_K$ in (6), define $\widehat{\mathbf{U}}_K^\mathsf{T} = [\widehat{\mathbf{U}}[e^{j\widetilde{\omega}_1}]^\mathsf{T} \dots \widehat{\mathbf{U}}[e^{j\widetilde{\omega}_K}]^\mathsf{T}]$. The block diagonal form of $\mathbf{H}_K$ and additive property of the ℓ_1-norm allow us to compute $\widehat{\mathbf{U}}[e^{j\widetilde{\omega}_l}]$ in a distributed fashion:

$$\widehat{\mathbf{U}}[e^{j\widetilde{\omega}_l}] = \underset{\mathbf{U}\in\mathbb{C}^{m\times 1}}{\arg\min} \left\{ \frac{1}{2} \left\| \mathbf{Y}[e^{j\widetilde{\omega}_l}] - \mathbf{H}[e^{j\widetilde{\omega}_l}]\mathbf{U} \right\|_2^2 + \lambda \|\mathbf{U}\|_1 \right\}.$$

The above optimization problem is computationally convenient and extremely useful to quickly determine the sources injecting oscillations with a particular frequency of interest.

To solve (7), we need $\mathbf{H}_K$, $\mathbf{Y}_K$, and K. The matrix $\mathbf{H}_K$ is computed using the power system matrices $(\mathbf{A}_d, \mathbf{B}_d, \mathbf{C})$. If these matrices not available, we can use empirically determined transfer functions obtained using system identification methods [9]. To compute K and $\mathbf{Y}_K$, we obtain the vector-valued N-point DFT[4] of $\mathbf{y}[L], \dots, \mathbf{y}[N-1+L]$ using

$$\widetilde{\mathbf{Y}}[q] \triangleq \frac{2}{N} \sum_{k=L}^{N-1+L} \mathbf{y}[k] e^{-j\frac{2\pi lk}{N}} \quad (q = 0, 1, \dots, N-1) \quad (8)$$

where we choose $L \gg 0$ such that $\mathbf{y}[k]$, for all $k \geq L$, is in steady state. For any q, recall that $\|\widetilde{\mathbf{Y}}[q]\|_\infty = \max_i |\widetilde{\mathbf{Y}}^{(i)}[q]|$, where $\widetilde{\mathbf{Y}}^{(i)}[q]$ is the i^{th} scalar in $\widetilde{\mathbf{Y}}^{(i)}[q] \in \mathbb{C}^p$.

The input (angular) frequencies can be determined using $\widetilde{\omega}_l = 2\pi l/N$, where l satisfies $\|\widetilde{\mathbf{Y}}[l]\|_\infty \neq 0$. However, due to the sensor noise and spectral leakage, $\|\widetilde{\mathbf{Y}}[l]\|_\infty$ could be non-zero even when $\widetilde{\omega}_l$ is not the true input frequency. The noise can be attenuated by filtering the measurements. Instead, we reduce spectral leakage by multiplying measurements with the Hamming window [14]. For these processed measurements, let $S = \{l : \|\widetilde{\mathbf{Y}}[l]\|_\infty > \tau\}$, where $\tau > 0$ is the user-defined threshold. Then $K = |S|$, where $|\cdot|$ is the cardinality of the set S, gives us the total number of input frequencies. Finally, we replace $\mathbf{Y}[e^{j\widetilde{\omega}_l}]$ in $\mathbf{Y}_K$ (given by (6)) with $\widetilde{\mathbf{Y}}[l]$, and evaluate the corresponding $\mathbf{H}[e^{j\widetilde{\omega}_l}]$ at $\widetilde{\omega}_l = 2\pi l/N$, where $l \in S$.

With $\mathbf{H}_K$ and $\mathbf{Y}_K$ at our disposal, we now can solve (7) using coordinate descent method [8] in the complex domain. We summarize our source recovery method in Algorithm 1, which recovers locations, and input parameters in discrete-time domain. We obtain the continuous-time frequency as $f_l = \widetilde{\omega}_l/(2\pi T)$. Instead, we recover amplitudes by $|\widehat{\mathbf{U}}_K|/\pi$, where $|\cdot|$ is the complex magnitude, applied for entry in $\widehat{\mathbf{U}}_K$.

Algorithm 1: Source localization via complex-LASSO

Input: $\tau > 0$, $\lambda \geq 0$, $\{\mathbf{Y}[k]\}_{k=L}^{N-1-L}$, and $(\mathbf{A}_d, \mathbf{B}_d, \mathbf{C})$.
Step 1: Compute $\widetilde{\mathbf{Y}}[q]$ using (8) and process them using the Hamming window.
Step 2: Set $S = \{l : \|\widetilde{\mathbf{Y}}[l]\|_\infty > \tau\}$ and $K = |S|$.
Step 3: Let $\mathbf{Y}_K = [\widetilde{\mathbf{Y}}[l_1] \dots \widetilde{\mathbf{Y}}[l_K]]$. Evaluate $\mathbf{H}[e^{j\widetilde{\omega}_{l_i}}]$ in (6) using $\widetilde{\omega}_{l_i} = 2\pi l_i/N$, and $l_i \in S$.
Step 4: Solve complex-LASSO problem in (7) using the coordinate descent method [8].
Return: $\widetilde{\omega}_l$; $\widehat{\mathbf{U}}[e^{j\widetilde{\omega}_l}]$; and source locations: indices of non-zero entries in $\widehat{\mathbf{U}}[e^{j\widetilde{\omega}_l}]$, $l = \{1, \dots, K\}$.

IV. Simulation Results

We apply Algorithm 1 to recover FO locations and oscillatory input parameters in two benchmark power systems. We add Gaussian noise with the SNR of 10 dB to the measurable quantities (see below). We let $1/T = F = 30$ and $N = 600$.

Tuning parameter (λ) selection: For $\lambda = 0$, the solution to (7) is given by the least squares solution. For $\lambda \geq \lambda_{\max} \triangleq \|\mathbf{Y}_K^T \mathbf{H}_K\|_\infty$, $\widehat{\mathbf{U}}_K = \mathbf{0}$ (a fully sparse vector) [8, Section 2.5]. Thus, we set $\lambda = \alpha\lambda_{\max}$ and choose $\alpha \in [0, 1]$ by performing a sensitivity analysis with respect to the true positive rate (TPR)—ratio of the number of correctly identified non-zero entries in $\widehat{\mathbf{U}}_K$ to the number of non-zero entries in $\mathbf{U}_K$—and the false positive rate (FPR)—ratio of the number of incorrectly identified non-zero entries in $\widehat{\mathbf{U}}_K$ to the number

[4]In simulations, for computational speedup, we use the FFT.

Israel-US BIRD Foundation

978-1-6654-0823-3/22/$31.00 ©2022 IEEE

of non-zero entries in $\mathbf{U}_K$. TPR and FPR depend on the noisy measurements and so does α. Thus to get a reliable and trustworthy α, we perform sensitivity analysis for 20 realizations of $\{y[k]\}_{k=L}^{N-1+L}$. We then pick an α that yields TPR $= 1$ and FPR $= 0$ for as many realizations as possible.

A. Case 1: IEEE 68 bus, 16 machine system [15]

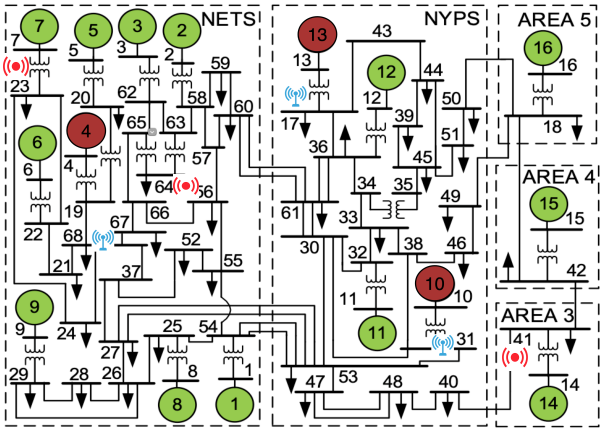

Fig. 4. IEEE NETS/NYPS 16 machine 68 bus system [15]. Among $m = 16$ excitation control inputs (green circles), only $m^* = 3$ locations (red colored bus no.s: 4, 10, 13) are excited by FO inputs.

Each generator is represented by ten states: the rotor angle, angular frequency, damper winding flux leakages, and states corresponding to excitation systems. We obtain the state space matrices using the power system toolbox (PST) [16]. See Fig. 4 and Table I for the inputs' description. We consider scenarios where PMUs are near and far away from the sources. For the first, PMUs are at buses 68, 31, and 17 (highlighted with a blue sensor icon in Fig. 4). For the latter, we place PMUs at buses 23, 41, and 64 (highlighted with a red sensor icon in Fig. 4). For all realizations, we correctly determined the input frequencies by thresholding the power spectrum of the voltage magnitude measurements (near and far case). Fig. 2 shows the spectrum of an arbitrary measurement realization.

The sensitivity analysis of the parameter α in terms of TPR and FPR for the two scenarios are shown in Fig. 3 (a) and (b), respectively. Due to space limitations, we focus only on nearby PMUs scenario. For $0.08 \leq \alpha \leq 0.14$, we were able to accurately find true FO locations in most of the realizations. Finally, for $\alpha = 0.14$, we report average and standard deviation of estimated input parameters in Table I.

B. Case 2: Reduced WECC 179 bus 29 machine system [17]

Each generator is modeled as a second order classical model and has two states: rotor angle and angular frequency. We use the small signal analysis tool (SSAT) to extract state space matrices of the WECC model described in [17]. We add FO input signals (parameters reported in Table I) to the mechanical torque of three generators at buses, labeled 5, 14, and 27 in [17, Fig. 1]. The PMU buses are 4, 18, and 47. Our measurements consist of the rotor angle of generators [10]. Fig. 3 (c) illustrates the sensitivity analysis of the parameter α in terms of TPR and FPR. Note that for $\alpha = 0.11$, we found the correct source locations.

V. Conclusions

This paper studies the effectiveness of complex-LASSO for source localization and input parameters estimation. Our problem formulation in the frequency domain clearly shows the sparsity in the number of locations and the number of sinusoids at a location. Thus, we cast the localization problem as an ℓ_1-regularized least squares problem, which we solve numerically via a complex-valued coordinate descent method. Our localization Algorithm 1 is simple and has a potential to be integrated into real-time grid operations. For simplicity, we present our results assuming the knowledge of dynamic models. However, our approach can even work with empirically determined transfer functions, and leave this study for future research. We plan also to compare our method to that of dissipating energy flow methods and data-driven approaches.

References

[1] M. Ghorbaniparvar. Survey on forced oscillations in power system. *J. of Modern Power Systems and Clean Energy*, 5(5):671–682, 2017.

[2] H. Ye et al. Analysis and detection of forced oscillation in power system. *IEEE Trans. Power Syst.*, 32(2):1149–1160, 2017.

[3] K. Manohar, J. N. Kutz, and S. L. Brunton. Optimal sensor and actuator selection using balanced model reduction. *IEEE Trans. Autom. Control*, pages 1–1, 2021.

[4] B. Wang and K. Sun. Location methods of oscillation sources in power systems: a survey. *J. of Modern Power Sys. and Clean Energy*, 5(2):151–159, 2017.

[5] J. A. Tropp and S. J. Wright. Computational methods for sparse solution of linear inverse problems. *Proceed. of the IEEE*, 98(6):948–958, 2010.

[6] T. Huang, N. M. Freris, P. R. Kumar, and L. Xie. A synchrophasor data-driven method for forced oscillation localization under resonance conditions. *IEEE Trans. on Power Systems*, 35(5):3927–3939, 2020.

[7] R. Anguluri, O. Kosut, and L. Sankar. Localization and estimation of unknown forced inputs: A group LASSO approach. *IEEE Transactions on Control of Network Systems*. Submitted.

[8] J. H. Friedman, T. Hastie, and R. Tibshirani. Regularization paths for generalized linear models via coordinate descent. *Journal of Statistical Software*, 33(1):1–22, 2010.

[9] N. Zhou, M. Ghorbaniparvar, and S. Akhlaghi. Locating sources of forced oscillations using transfer functions. In *2017 IEEE Power and Energy Conference at Illinois (PECI)*, pages 1–8. 2017.

[10] M. Luan, S. Li, D. Gan, and D. Wu. Frequency domain approaches to locate forced oscillation source to control device. *International Journal of Electrical Power & Energy Systems*, 117:105704, 2020.

[11] S. Roy, W. Ju, N. Nayak, and B. Lesieutre. Localizing power-grid forced oscillations based on harmonic analysis of synchrophasor data. In *55th Annual Conference on Information Sci. and Sys.*, pages 1–5, 2021.

[12] S. C. Chevalier, P. Vorobev, and K. Turitsyn. Using effective generator impedance for forced oscillation source location. *IEEE Trans. Power Syst.*, 33(6):6264–6277, 2018.

[13] S. C. Chevalier, P. Vorobev, and K. Turitsyn. A bayesian approach to forced oscillation source location given uncertain generator parameters. *IEEE Trans. Power Syst.*, 34(2):1641–1649, 2019.

[14] P. Stoica and R. Moses. *Introduction to Spectral Analysis*. Upper Saddle River, NJ: Prentice-Hall, 1997.

[15] A. K. Singh et al. Report on the 68-bus, 16-machine, 5-area system. *IEEE PES Task Force on Benchmark Systems for Stability Controls. Ver*, 3, 2013.

[16] J.H. Chow and K.W. Cheung. A toolbox for power system dynamics and control engineering education and research. *IEEE Transactions on Power Systems*, 7(4):1559–1564, 1992.

[17] S. Maslennikov et al. A test cases library for methods locating the sources of sustained oscillations. In *2016 IEEE Power and Energy Society General Meeting (PESGM)*, pages 1–5, 2016.

Israel-US BIRD Foundation

978-1-6654-0823-3/22/$31.00 ©2022 IEEE

TABLE I

TRUE AND ESTIMATED VALUES OF THE AMPLITUDE, FREQUENCY AND PHASE OF THE FORCED OSCILLATIONS INPUTS

System under study	FO Location	Input Signal								
		Amplitude (p.u.)			Frequency (Hz)			Phase (rad)		
		Parameter	True	Estimate (σ)*	Parameter	True	Estimate	Parameter	True	Estimate (σ)*
68-bus system (near PMUs)	4	$a_{4,1}$	0.01	0.0126 (0.003)	$f_{4,1}$	2	2	$\phi_{4,1}$	0.3	0.3302 (0.024)
		$a_{4,2}$	0.01	0.0081 (0.0018)	$f_{4,2}$	2.5	2.5	$\phi_{4,2}$	0.4	0.4401 (0.012)
	10	$a_{10,1}$	0.01	0.0087 (0.005)	$f_{10,1}$	1.5	1.5	$\phi_{10,1}$	0.1	0.1326 (0.01)
		$a_{10,2}$	0.01	0.0093 (0.006)	$f_{10,2}$	1	1	$\phi_{10,2}$	0.3	0.2804 (0.024)
	13	$a_{13,1}$	0.02	0.0169 (0.004)	$f_{13,1}$	3.5	3.5	$\phi_{13,1}$	0.1	0.0893 (0.007)
		$a_{13,2}$	0.02	0.0170 (0.002)	$f_{13,2}$	0.8	0.8	$\phi_{13,2}$	0.2	0.1771 (0.0052)
WECC-179 bus system	5	$a_{5,1}$	0.02	0.0244 (0.002)	$f_{5,1}$	1	1	$\phi_{5,1}$	0.3	0.2993 (0.0133)
		$a_{5,2}$	0.01	0.0117 (0.005)	$f_{5,2}$	0.8	0.8	$\phi_{5,2}$	0.4	0.3405 (0.0305)
	14	$a_{14,1}$	0.03	0.0214 (0.008)	$f_{14,1}$	0.7	0.7	$\phi_{14,1}$	0.2	0.2134 (0.0068)
		$a_{14,2}$	0.02	0.0170 (0.001)	$f_{14,2}$	1.5	1.5	$\phi_{14,2}$	0.3	0.2613 (0.0048)
	27	$a_{27,1}$	0.04	0.0350 (0.007)	$f_{27,1}$	2	2	$\phi_{27,1}$	0.1	0.1076 (0.0098)
		$a_{27,2}$	0.01	0.0094 (0.003)	$f_{27,2}$	1.2	1.2	$\phi_{27,2}$	0.2	0.2567 (0.0457)

* Standard deviation of estimated parameters over 20 realizations of noisy measurements.

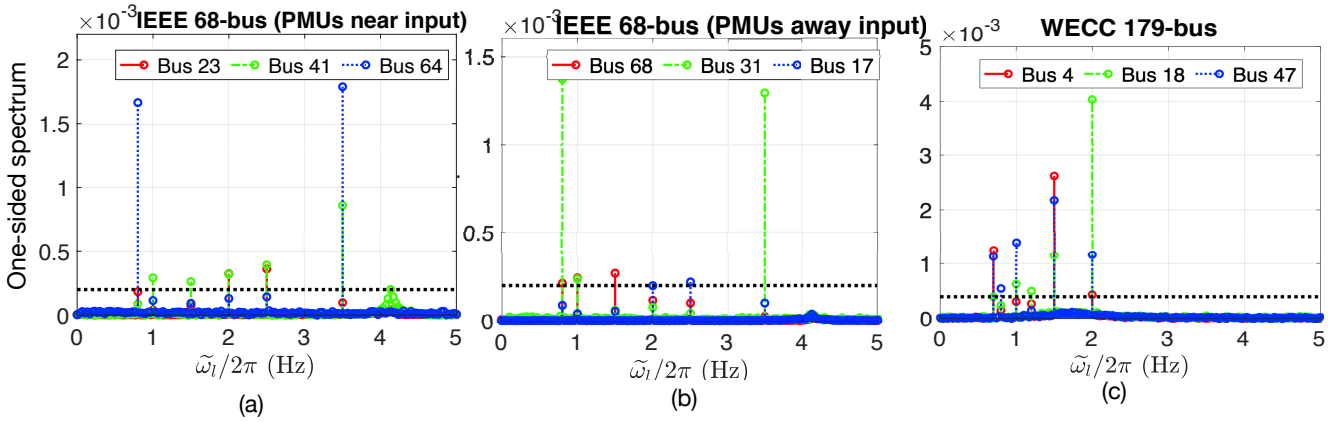

Fig. 2. One-sided power spectrum of measurements for different case studies. In each plot, we overlay the spectrum associated with different measurement buses. The black dashed line represents the thresholding parameter τ, which equals 0.2×10^{-3} in Fig. (a) and (b), and 0.4×10^{-3} in Fig. (c). Theoretically, if inputs are observable, the spectrum of each PMU measurement should contain dominant peaks at all input frequencies. However, as evident in all plots, not even for one PMU, we can see dominant peaks at all input frequencies. This can be attributed to the measurement noise and spectral leakage. However, by considering all PMUs, we see sharp dominant peaks at all input frequencies. Interestingly, for IEEE-68 bus case, the magnitude of spectral peaks is smaller when PMUs are away from the true source locations. Thus it makes sense to consider measurements from nearby PMUs if we have prior coarse knowledge of source locations.

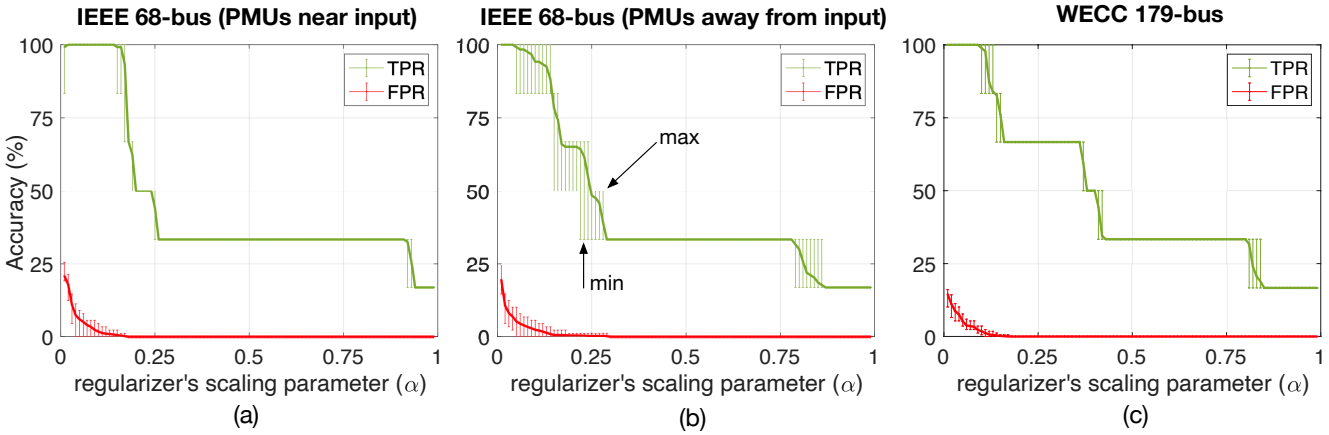

Fig. 3. Sensitivity analysis of the scaling parameter α in terms of TPR and FPR for different cases. The error bars in the figures illustrate the maximum and minimum of twenty values (as described in the main text) of TPR and FPR. Instead, the solid line is the average value Interestingly, from panels (a) and (b), we note that the PMUs in the vicinity of the FO sources resulted in a wider range of α values that yield a better TPR (100%) and FPR (0%).

978-1-6654-0823-3/22/$31.00 ©2022 IEEE